Proc. of the 6th Intl. Symposium on Reliability Engineering and Risk Management (6ISRERM)
31 May – 1 June 2018, Singapore
Editor(s) Xudong Qian, Sze Dai Pang, Ghim Ping Raymond Ong, Kok-Kwang Phoon

Prediction of the extreme air gap response in semi-submersible floating structures

Zizhe Wang[1] and Ying Min Low[2]

[1]*Department of Civil and Environmental Engineering, National University of Singapore, 1 Engineering Drive 2, Singapore 117576, Singapore.*
E-mail:zizhe.wang@u.nus.edu
[2]*Department of Civil and Environmental Engineering, National University of Singapore, 1 Engineering Drive 2, Singapore 117576, Singapore.*
E-mail: ceelowym@nus.edu.sg

Airgap is a crucial design consideration of semi-submersible floating structures, which is defined as the clearance between the platform deck and wave surface. Consequently, the platform motion and wave elevation are both important for airgap analysis. Furthermore, the nonlinearity of them enables airgap response to have evident non-Gaussian characteristics, which makes the prediction of extreme airgap response intricate. In this paper, a coupled analysis of the airgap response is performed. The software HydroStar is used to model the wave-structure interaction and construct the linear transfer functions and quadratic transfer functions for wave forces in irregular seastate. Then the platform motion and wave elevation are analyzed simultaneously in the time domain to get the airgap response, the nonlinear damping effect is incorporated during this process. Then an extreme analysis is carried out based on the time domain results. This study shows that the low-frequency (LF) roll and pitch motions of the platform increase the nonlinearity of the airgap response, especially for the points located at the edge of platform deck. Besides, the LF component of airgap response trends to increase the extreme value.

Keywords: Airgap, Semi-submersible, Low-frequency motion, Extreme prediction.

1 Introduction

The semi-submersible floating structure is extensively used for drilling and production of the offshore oil resources. Its platform consists of several horizontal pontoons supporting an elevated rectangular deck by a number of vertical columns. This concept reduces the wave-structure interactions and provides good motion characteristics. For the design of semi-submersible floating structures, the airgap is a key design consideration. It is defined as the vertical clearance between the lower deck and corresponding water surface. The wave will slam on the lower deck once the airgap decreases to zero, which may give rise to a series of problems and eventually cause the failure of offshore structures. For instance, the accident happened in North Sea COSL Innovator platform on 30th Dec 2015 is caused by a huge wave slamming on the platform. This accident killed one worker and injured two others (Schuler, 2015). On the other hand, overestimation of the airgap will make the cost increase substantially. Therefore the accurate prediction of the extreme airgap response is curial for the design of semi-submersible floating structures.

The airgap analysis has been topical for many years. As the airgap response consists of the vertical platform motion and corresponding wave elevation, different researchers focused on different aspects. The pioneer work done by Sweetman *et al.* (2001) focused on the second order wave amplification effect due to the presence of platform in the random sea state. They carried out the second order diffraction analysis in WAMIT and computed Quadratic Transfer Function (QTF) for the wave amplification. However, the QTF at low period was excessive, which led to overestimation of wave amplification effect. Thus they proposed to cut off the QTF before a certain period and substitute with Stokes Theory. This post-processing method was further validated by using the system identification method to get the QTF from experimental data (Sweetman *et al.*, 2002). Kazemi and Incecik (2007) carried out a series of studies on airgap response under regular waves. They found significant wave amplification occurred at the mid-point between two columns which are parallel to the incident wave. Besides, the evident wave run-up effect was found at vicinity of column. This run-up effect is a local response that cannot be modeled by the diffraction analysis. Stansberg *et al.* (2005) and Matsumoto *et al.* (2013) used the Volume of Fluid CFD code to simulate wave run-up, and the result matched quite well with model test.

Previous studies have made significant progress and provided insights into the airgap problem. However, the limitations of past research and complexity of airgap problem warrant further investigation. For instance, most of the previous studies focused on one aspect of airgap response, while the actual response is a coupled process of the platform motion and wave elevation. These two processes should be analyzed simultaneously to incorporate their phase relationship. In addition, recently studies showed that there are significant low frequency (LF) roll and pitch motions of semi-submersible (Matos *et al.*, 2011). These non-Gaussian LF motions increases the intricacy of the extreme prediction, and the research on the influence of LF motions on the extreme airgap response is scarce.

This paper aims to conduct an extreme analysis of the airgap response in random sea state. The nonlinear hydrodynamic analysis was performed firstly to construct the Linear Transfer Function (LTF) and Quadratic Transfer Function (QTF) for the wave excitation forces. Then structural dynamic analysis was carried out in the time domain to calculate the platform motions. The nonlinear spatial-variant wave elevation was also evaluated to compute the actual time series of the airgap response at the different airgap probes. An upcrossing analysis was performed based on the time domain results to predict the extreme values.

2 Nonlinear Hydrodynamic Analysis

The nonlinear hydrodynamic analysis was performed by HydroStar, which is a state-of-art hydrodynamic software developed by Bureau Veritas. This software is based on the potential flow theory and adopts the Boundary Element Method for the numerical computation. In this project, an unnamed semi-submersible with four circular columns and two rectangular pontoons was selected. The key platform dimensions and test conditions are listed in Table 1.

Based on the dimensions and test conditions, a three-dimensional mesh model with six degree-of-freedoms was built in the HydroStar, as shown in Figure 1. Normally only the submerged part of the platform is required to be modeled. In addition, a large amount of panels is required for the components near the mean water level since wave-structure interactions occur mostly at the free surface level. The mesh model includes 5754 panels in total, which is assumed to be sufficient for numerical convergence and stability. Besides, the blue part in Figure 1 is the bracing member. Because the diameter of bracing member is usually small and the fictitious effect cannot be neglected, the bracing member is modeled as Morison members. The wave frequencies are defined from 0 rad/s to 1.2 rad/s with equal width $\Delta\omega$=0.005rad/s. LTF for first

order wave frequency (WF) forces and first order wave elevation, QTF for second order low frequency (LF) forces were constructed after the diffraction analysis.

Table 1. **Platform dimensions and test conditions**

Platform dimension	Value	Test condition	Value
Overall length	105.00 m	Draft	18.5 m
Width outside pontoons	64.50 m	Water depth	1000 m
Pontoon length	93.50 m	Displacement	28650 tons
Pontoon width	14.00 m	Center of gravity (from keel)	18.34 m
Pontoon height	8.625 m	Still water airgap	12 m
Column diameter	14.00 m	GM, transverse	2.268 m
Column height	21.875 m	GM, longitudinal	2.547 m
Column spacing, longitudinal	51.00 m	Roll radius of gyration	27.5 m
Column spacing, transverse	50.50 m	Pitch radius of gyration	29.6 m
Bracing member length	36.5 m	Yaw radius of gyration	33.4 m

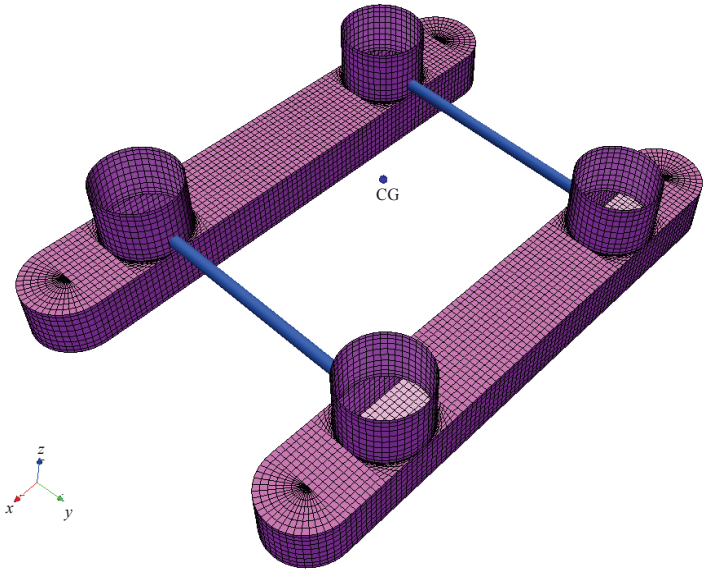

Figure 1. Semi-submersible mesh in Hydrostar

3 Dynamic Analysis and Airgap Analysis in Time Domain

Based on the transfer function from Hydrostar, the dynamic analysis was carried out in time domain to compute the time history of global platform motions (i.e. surge, sway, heave, roll, pitch, and yaw). The time history of first order wave excitation force $F^{(1)}(t)$ and second order wave excitation force $F^{(2)}(t)$ were pre-generated by:

$$F^{(1)}(t) = \mathrm{Re}\sum_{n=1}^{N} LTF(\omega_n) A_n \exp(i\omega_n t) \tag{1}$$

$$F^{(2)}(t) = \mathrm{Re}\sum_{n=1}^{N}\sum_{m=1}^{N} QTF(\omega_n, \omega_m) A_n A_m^* \exp\left[i(\omega_n - \omega_m)t\right] \tag{2}$$

$$A_n = a_n \exp(i\varepsilon_n) \tag{3}$$

where A_n is the complex wave amplitude that contains the random phase information. Here a_n should be randomly chosen from Rayleigh distribution with mean square of $2S_{\eta\eta}(\omega_n)\Delta\omega$, and random phase ε_n is distributed evenly from 0 to 2π. The JONSWAP spectrum with significant wave height 13.5m and zero-crossing period 13.5s was applied in this project. Equations (1) and (2) can be evaluated efficiently by the inverse Fast Fourier Transform (FFT) techniques.

After the time series of the wave excitation forces were generated, the dynamic analysis was carried out in the time domain. The Newmark-β method was implemented to solve the equation of motion step by step. As the diffraction analysis is based on the assumption that the flow is inviscid, incompressible and irrotational, the viscous effect should be considered during the dynamic analysis. In this project, drag forces acting on the submerged part of platform were updated at each time step to model the nonlinear viscous effect. Following this procedure, the time history of global motions of the platform was obtained.

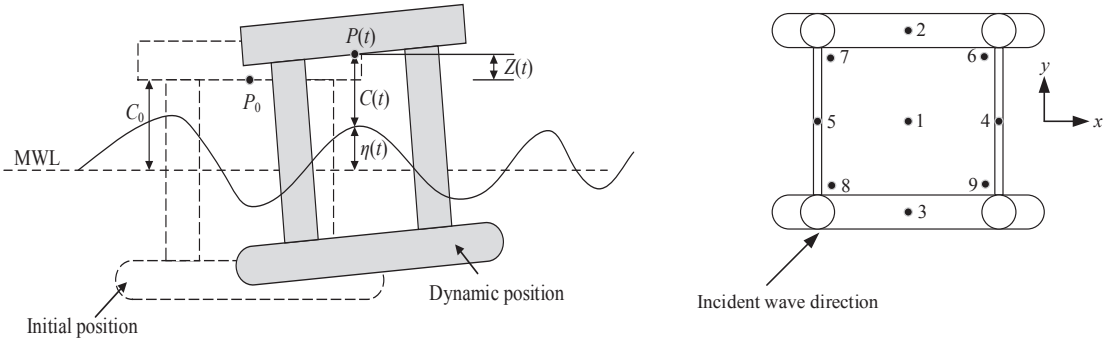

Figure 2. Schematic of airgap & location of airgap probes

After the dynamic analysis of the platform, the time history of the airgap response can be evaluated. According to the schematic view of the airgap in Figure 2, the airgap response $C(t)$ can be written as:

$$C(t) = C_0 + Z(t) - \eta(t) \tag{4}$$

where C_0 denotes the still water airgap, which is the clearance between the lower deck at still state and mean water level (MWL). The vertical displacement of the airgap probe is denoted as $Z(t)$, corresponding wave elevation is $\eta(t)$. Consider a airgap probe with local position $\mathbf{p}=[p_x\ p_y\ p_z]^T$, the vertical motion $Z(t)$ can be obtained from the rotation matrix:

$$Z(t) = \xi_z + p_y\varphi_x - p_x\varphi_y \tag{5}$$

Therefore, vertical displacement is a coupled process of heave ξ_z, roll φ_x and pitch φ_y. Besides, the horizontal displacement of the airgap probe was also calculated to get the spatial variant wave elevation at each time step. The wave elevation is expressed as:

$$\eta(t) = \eta_{1,i}(t) + \eta_{1,d}(t) + \eta_{1,r}(t) + \eta_{2,i}(t) \tag{6}$$

where the $\eta_{1,i}(t)$, $\eta_{1,d}(t)$ and $\eta_{1,r}(t)$ are the first order incident wave, diffracted wave, and radiated wave respectively. HydroStar can provide the transfer functions for these first order waves. The second order stokes wave theory was implemented to evaluate the second order incident wave $\eta_{2,i}(t)$. Thereafter, the time history of the airgap response was obtained.

As shown in Figure 2, nine airgap probes were installed on the platform. As the wave slamming effect often occurred at the region near the column (Kazemi & Incecik, 2007; Sweetman *et al.*, 2001), some probes were placed there (probe 6, 7, 8, 9). In addition, the volume of the pontoon is considerately large such that some probes were placed above the pontoon to analyze the diffraction effect of the pontoon (probe 2, 3, 4, 5).

The time history of the dynamic response of the probe 1 is plotted in Figure 3, where the blue solid line represents the vertical position of the probe, and the red dash line represents the corresponding wave elevation. Therefore, the airgap response is the difference between these two lines and the intersection of them represents a wave slamming event. Figure 3 indicates that the vertical displacement and wave elevation have the correlation effect, which means that these two processes are coupled and should be analyzed simultaneously. However, most of the previous research overlooked this correlation effect.

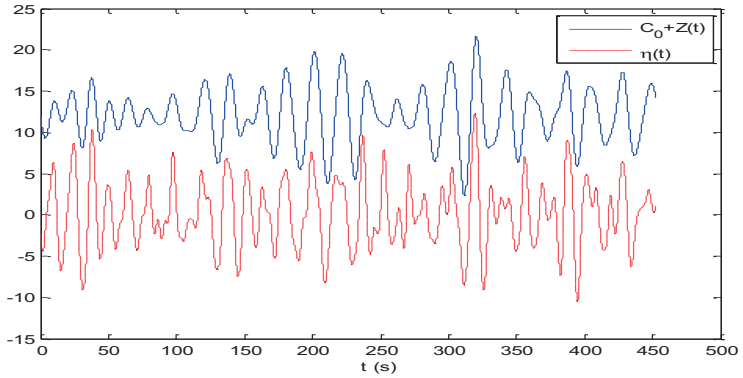

Figure 3. Time history of vertical position and wave elevation (Probe 1)

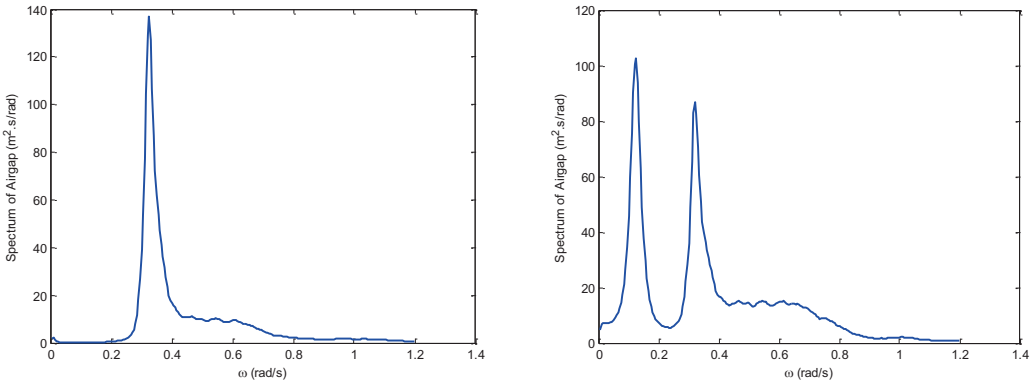

Figure 4. Spectrum of the airgap response (left: probe1; right probe 6)

Apart from the time history of the airgap response, the spectrum of airgap response was recovered from time history and plotted in Figure 4. It is interesting to find that the shapes of spectrum is related to the position of airgap probes. For example, the spectrum of the airgap response at probe 1 has only one peak and it is mainly distributed along the wave frequency range (0.2rad/s-1.2rad/s). However, the spectrum of the airgap response at probe 6 has two peaks, one is at the low frequency range (0rad/s-0.2rad/s) and the other one is at the wave frequency range. Furthermore, the standard deviation of the airgap response calculated from the spectrum confirms this phenomena, as shown in Table 2. This phenomena may due to the LF roll and pitch motions of the platform, which will be explained as follows. For the probe 1, it is located in the center of the platform, so that its vertical displacement is purely heave motion. For the probes located off the center of the platform, their vertical displacements are related to the

heave, roll, and pitch motions. Therefore the LF roll and pitch motion contributes to the final airgap response at the probes off the center of the platform. This contribution makes the spectrum of the airgap response has a peak at the LF range, as shown in Figure 4. This phenomena indicates that the airgap response of semi-submersible has the significant nonlinearity since the LF roll and pitch motions is nonlinear.

Table 2. Standard deviation of the airgap response

Airgap probe	LF component (m)	WF component (m)
Probe 1	0.2720	3.2810
Probe 2	1.7745	3.3046
Probe 3	1.6174	3.7501
Probe 4	1.7017	3.0336
Probe 5	1.5257	3.5146
Probe 6	2.4187	3.3771
Probe 7	0.5528	3.2607
Probe 8	2.2414	3.9249
Probe 9	0.5761	3.2831

4 Extreme Analysis of Airgap Response

As aforementioned, the LF roll and pitch motions have significant influence on airgap response. Thus their influence on the extreme airgap response was also investigated in this section. A Monte Carlo simulation was carried out to get the sufficient results of time history of airgap response. Then an upcrossing analysis was performed for the extreme analysis of airgap response.

The design philosophy of semi-submersible is to maintain the lower deck above the wave surface. Therefore the limited state of airgap responses is zero airgap and occurrence of wave impact, expressed as:

$$C(t) = C_0 + Z(t) - \eta(t) > 0 \tag{7}$$

However, if this formula is used for extreme analysis, the crossing rate analysis is actually the downcrossing rate analysis. Therefore, this formula is transformed into another expression in order to carry our the upcrossing rate analysis, which can be written as:

$$R_w(t) = \eta(t) - Z(t) < C_0 \tag{8}$$

where $R_w(t)$ is the relative wave elevation. The relative wave elevation should be smaller than still water airgap C_0, thus ensures the implementation of upcrossing analysis.

The basic procedure of upcrossing analysis is to count the number of upcrossing event within the time duration T. The upcrossing event is defined as the process crossing a certain threshold with positive slope. Then the upcrossing rate can be written as:

$$\nu_b^+ = \frac{n_b^+(b;T)}{T} \tag{9}$$

where b is the threshold, n is the number of upcrossing event.

The upcrossing rates of airgap reponses at different probes are plotted in Figure 5. In order to show the non-Gaussian charteristics of the airgap response, the upcrossing rate of the equivalent Gaussian process that shares the same standarad deviation is also plotted.

In Figure 5, the red solid line is the upcrossing rate generated from the time history, and the black dash line is the upcrossing rate of the equivalent Gaussian process, which is also a linear process. For the upcrossing rate of airgap response at probe 1, the red line and black line match quite well, which indicates that the extreme airgap response at the center of the platform can be

predicted by the common linear process. However, for the probe 6, the red line exceeds the black line as the threshold increases, which indicates that the upcrossing rate of the airgap response at probe 6 is higher than that of linear process. In addition, the higher upcrossing rate represents the larger extreme value. Therefore, the LF roll and pitch motions trend to increase the extreme airgap response at the probes off the center of the platform.

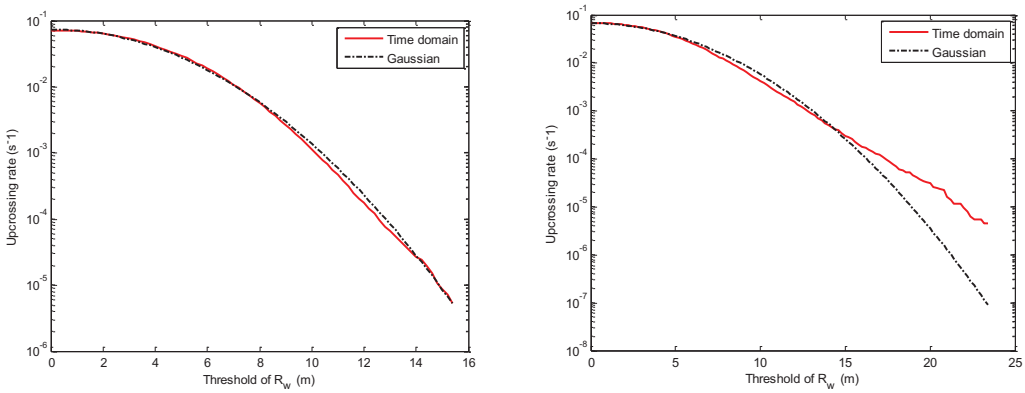

Figure 5. Upcrossing rate of the airgap response (left: probe1; right probe 6)

5 Conclusions and Future Work

An extreme analysis of the airgap response of semi-submersible floating structure was carried out in this paper. The nonlinear platform motion and spatial variant wave elevation were evaluated simultaneously to get the time history of the airgap responses. The results showed that airgap response is a coupled process such that the platform motion and wave elevation must be analyzed simultaneously. Besides, the LF component in roll and pitch motions makes airgap responses at the off-center points have evident LF component. These LF components contribute to the non-Gaussian characteristics of airgap response vastly. The upcrossing analysis shows that LF components trend to increase the extreme value of the airgap response. Thus the conventional Gaussian assumption will underestimate the probability of failure.

The time domain simulation adopted in this paper is quite time-consuming. In addition, the Monte Carlo simulation is very hard to predict the extreme values with small crossing rate. Progressive research is required to develop the efficient extreme prediction method of airgap response of semi-submersible floating structures.

Acknowledgments

This study is funded by the NUS industry ring-fenced Research Scholarship, in collaboration with Bureau Veritas. The authors are grateful to Bureau Veritas for providing access to the software HydroStar as well as guidance from the industry perspective.

References

Kazemi, S., & Incecik, A., Theoretical and experimental analysis of air gap response and wave-on-deck impact of floating offshore structures, in *26th International Conference on Offshore Mechanics and Arctic Engineering*, 297-304, San Diego, California, USA, 2007.

Matos, V. L. F., Simos, A. N., & Sphaier, S. H., Second-order resonant heave, roll and pitch motions of a deep-draft semi-submersible: Theoretical and experimental results, *Ocean Engineering*, 38(17), 2227-2243, 2011.

Matsumoto, F. T., Watai, R. A., Simos, A. N., & Ferreira, M. D., Wave Run-Up and Air Gap Prediction for a Large-Volume Semi-Submersible Platform, *Journal of Offshore Mechanics and Arctic Engineering*, 135(1), 011302, 2013.

Schuler, M. One Dead, Two Injured After Wave Hits North Sea Drilling Rig COSL Innovator. Retrieved from http://gcaptain.com/three-injured-aboard-north-sea-oil-rig-during-storm-frank/, December 30, 2015.

Stansberg, C. T., Baarholm, R., Kristiansen, T., Hansen, E. W. M., & Rortveit, G., Extreme wave amplification and impact loads on offshore structures, in *Offshore Technology Conference*, 2005.

Sweetman, B., Winterstein, S. R., & Cornell, C. A., Airgap analysis of floating structures: first-and second-order transfer functions from system identification, *Applied ocean research*, 24(2), 107-118, 2002.

Sweetman, B., Winterstein, S. R., Meling, T. S., & Birknes, J., Airgap Prediction: Use of Second-Order Diffraction and Multi-Column Models, in *The Eleventh International Offshore and Polar Engineering Conference*, 2001.